Co-localised phosphorus mobilization processes in the rhizosphere of field-grown maize jointly contribute to plant nutrition

Nataliya Bilyera, Christina Hummel, Gabrielle Daudin, Michael Santangeli, Xuechen Zhang, Jakob Santner, Eva Lippold, Steffen Schlüter, Isabelle Bertrand, Walter Wenzel, et al.

▶ **To cite this version:**

Nataliya Bilyera, Christina Hummel, Gabrielle Daudin, Michael Santangeli, Xuechen Zhang, et al.. Co-localised phosphorus mobilization processes in the rhizosphere of field-grown maize jointly contribute to plant nutrition. Soil Biology and Biochemistry, 2022, 165, pp.108497. 10.1016/j.soilbio.2021.108497 . hal-03479348

HAL Id: hal-03479348
https://hal.inrae.fr/hal-03479348

Submitted on 14 Dec 2021

HAL is a multi-disciplinary open access archive for the deposit and dissemination of scientific research documents, whether they are published or not. The documents may come from teaching and research institutions in France or abroad, or from public or private research centers.

L'archive ouverte pluridisciplinaire **HAL**, est destinée au dépôt et à la diffusion de documents scientifiques de niveau recherche, publiés ou non, émanant des établissements d'enseignement et de recherche français ou étrangers, des laboratoires publics ou privés.

Distributed under a Creative Commons Attribution 4.0 International License

Soil Biology and Biochemistry 165 (2022) 108497

Contents lists available at ScienceDirect

Soil Biology and Biochemistry

journal homepage: www.elsevier.com/locate/soilbio

Co-localised phosphorus mobilization processes in the rhizosphere of field-grown maize jointly contribute to plant nutrition

Nataliya Bilyera [a,b,1], Christina Hummel [c,1], Gabrielle Daudin [d], Michael Santangeli [c], Xuechen Zhang [e], Jakob Santner [f], Eva Lippold [g], Steffen Schlüter [g], Isabelle Bertrand [d], Walter Wenzel [c], Sandra Spielvogel [b], Doris Vetterlein [g,h], Bahar S. Razavi [a,**], Eva Oburger [c,*]

[a] Department of Soil and Plant Microbiome, Institute of Phytopathology, Christian-Albrechts-University of Kiel, 24118, Kiel, Germany
[b] Department of Soil Science, Institute for Plant Nutrition and Soil Science, Christian-Albrechts-University of Kiel, 24118, Kiel, Germany
[c] Department of Forest and Soil Science, Institute of Soil Research, University of Natural Resources and Life Sciences, Tulln, Austria
[d] Eco&Sols, Univ Montpellier, CIRAD, INRAE, IRD, Montpellier SupAgro, Montpellier, France
[e] Department of Biogeochemistry of Agroecosystems, University of Göttingen, 37077, Göttingen, Germany
[f] Institute of Agronomy, University of Natural Resources and Life Sciences, Tulln, Austria
[g] Department of Soil System Science, Helmholtz Centre for Environmental Research - UFZ, Theodor-Lieser-Strasse. 4, 06120, Halle/Saale, Germany
[h] Institute of Agricultural and Nutritional Sciences, Martin Luther University Halle-Wittenberg, Von-Seckendorff-Platz 3, 06120, Halle/Saale, Germany

ARTICLE INFO

Keywords:
Diffusive gradients in thin films (DGT)
Planar pH optodes
Root hairs
Root window
Soil texture
Soil zymography

ABSTRACT

Understanding phosphorus (P) dynamics in the rhizosphere is crucial for sustainable crop production. P mobilization processes in the rhizosphere include the release of plant and microbially-derived protons and extracellular phosphatases. We investigated the effect of root hairs and soil texture on the spatial distribution and intensity of P mobilizing processes in the rhizosphere of *Zea mays* L. root-hair defective mutant (*rth3*) and wild-type (WT) grown in two substrates (loam, sand). We applied 2D-chemical imaging methods in custom-designed root windows installed in the field to visualize soil pH (optodes), acid phosphatase activity (zymography), and labile P and Mn fluxes (diffusive gradients in thin films, DGT).

The average rhizosphere extent for phosphatase activity and pH was greater in sand than in loam, while the presence of root-hairs had no impact. Acidification was significantly stronger at young root tissue (<2 cm from root cap) than at older root segments (>4 cm from root cap) and stronger in WT than *rth3*. Accompanied with stronger acidification, higher P flux was observed mainly around young, actively growing root tissues for both genotypes. Our results indicate that acidification was linked to root growth and created a pH optimum for acid phosphatase activity, *i.e.*, mineralization of organic P, especially at young root tissues which are major sites of P uptake. Both genotypes grew better in loam than in sand; however, the presence of root hairs generally resulted in higher shoot P concentrations and greater shoot biomass of WT compared to *rth3*. We conclude that soil substrate had a larger impact on the extent and intensity of P solubilization processes in the rhizosphere of maize than the presence of root hairs. For the first time, we combined 2D-imaging of soil pH, phosphatase activity, and nutrient gradients in the field and demonstrated a novel approach of stepwise data integration revealing the interplay of various P solubilizing processes *in situ*.

1. Introduction

Phosphorus (P) is extremely immobile in soil and therefore often the growth-limiting nutrient. Understanding P mobilization mechanisms of roots and related dynamics in the rhizosphere is a prerequisite for exploiting poorly available, recalcitrant soil P, *i.e.*, P sorbed, precipitated or immobilized in organic forms (Pierzynski et al., 2005; Stutter et al., 2012). Plants can only take up soluble inorganic P (P_i, *i.e.* HPO_4^{2-} or $H_2PO_4^-$), which is present in soil solution in low concentrations due to its high reactivity and strong retention by the soil matrix (Pierzynski

* Corresponding author.
** Corresponding author.
E-mail addresses: brazavi@phytomed.uni-kiel.de (B.S. Razavi), eva.oburger@boku.ac.at (E. Oburger).
[1] These authors contributed equally to this work.

https://doi.org/10.1016/j.soilbio.2021.108497
Received 3 August 2021; Received in revised form 25 October 2021; Accepted 23 November 2021
Available online 28 November 2021
0038-0717/© 2021 The Authors. Published by Elsevier Ltd. This is an open access article under the CC BY license (http://creativecommons.org/licenses/by/4.0/).

et al., 2005). Organic P (P_o) can only be used by plants after enzyme-mediated conversion to phosphate via mineralization into soluble compounds (Jones and Oburger, 2011). Soil mineralogy and soil texture strongly influence P availability as P is precipitated as Ca, Fe, Al phosphates, or sorbed on Fe and Al (hydr)oxides, organic matter and clay minerals (Baldovinos and Thomas, 1967).

To overcome P deficiency, morphological root traits like higher root density and formation of root hairs increase the root surface to expand the area that is in contact with the exploitable soil and contribute to an up to 50% higher P uptake (Daly et al., 2016; Itoh and Barber, 1983; Ruiz et al., 2020).

If soil solution concentrations are too low, morphological adaptations might not be sufficient to meet the plants P demand (Gerke, 2015) and roots (bio)chemically modify their rhizosphere to render P more plant available and increase P_i uptake (George et al., 2018). Plant and microbially derived phosphatases, organic acids, and protons directly increase P availability due to mineralization of organic P to orthophosphate (Jones and Oburger, 2011; Sims and Pierzynski, 2005; Turner et al., 2002), ligand exchange (Bertrand et al., 1999; Jones, 1998), and mineral dissolution (Barrow, 2017; Barrow et al., 2020). In addition, root hairs were found to enlarge the rhizosphere extent for acid phosphatase activity (Holz et al., 2020; Ma et al., 2018) and cause P depletion (Gahoonia et al., 2001). Moreover, carbon from rhizo-deposits also indirectly increases P availability by stimulation of P solubilizing microorganisms to release phosphatases (Manzoor et al., 2017; Merbach et al., 2010; Whipps, 2001; Yang et al., 2017), thus facilitating rapid turnover of P immobilized in microbial biomass (Raymond et al., 2020; Turner et al., 2003). P solubilization processes such as acidification and carboxylate exudation can co-solubilize other nutrients such as manganese (Mn) (Lambers et al., 2015) resulting in co-localized, increased labile P and Mn concentrations in the rhizosphere (Kreuzeder et al., 2018).

Individual P solubilization processes in the rhizosphere might interact but are difficult to measure in intact soil. Non-destructive 2D imaging techniques enable to semi-quantitatively assess the spatiotemporal distribution of rhizosphere parameters at μm to mm scales (Oburger and Schmidt, 2016). For instance, planar optodes visualize pH patterns (Blossfeld and Gansert, 2007), zymography and colorimetric imaging assess the distribution of phosphatase activity (Dinkelaker and Marschner, 1992; Grierson and Comerford, 2000; Razavi et al., 2019; Spohn et al., 2013), and diffusive gradients in thin films (DGT) maps the distribution of the labile fraction of nutrients such as P (Kreuzeder et al., 2013). Particularly when combined, these imaging techniques allow unique insights into interactions of individual P solubilization processes (Hummel et al., 2021; Kreuzeder et al., 2018; Ma et al., 2018, 2021). Rhizoboxes provide easy access to roots and rhizosphere soil and facilitate the application of imaging techniques in the laboratory (Kuzyakov and Razavi, 2019; Neumann et al., 2009; Oburger and Schmidt, 2016), however such laboratory-based studies are often limited to early-plant developmental stages and consequently spatiotemporal information on rhizosphere parameters of mature plants is scarce. Permanently installed flat root windows enable non-destructive sampling across plant development *in situ* under field conditions (Dong et al., 2007; Hahn and Marschner, 1998; Marschner et al., 1991; Stober et al., 2000), but, to the best of our knowledge, (bio)chemical imaging techniques for pH, phosphatase activity and labile nutrients have not yet been performed and combined under field-conditions in croplands.

Here we investigated the interplay of two P solubilization processes (e.g., acidification and mineralization of organic P to phosphate) by combining planar optodes, zymography and DGT imaging under field conditions using custom-made root windows, which enable non-destructive and repeated sampling *in situ*. Two *Zea mays* L. genotypes, *i.e.*, a root-hair forming wild-type and root-hair defective mutant *rth3*, were grown on two substrates with contrasting textures (sand and loam) (Vetterlein et al., 2021). Due to lower total P and fewer sorption sites in sand than in loam, we hypothesized that the lower P and pH buffer capacity in sand will induce stronger rhizosphere acidification and higher phosphatase activity consequently resulting in a larger rhizosphere extent of both parameters combined with stronger P depletion gradients in sand compared to loam. Furthermore, we expected that root hairs not only enlarge the absorption surface for nutrients (Jungk, 2001) but also enhance the rhizosphere extent for acidification, phosphatase activity, and P depletion compared to root-hair defective *rth3* irrespective of soil texture. We applied different strategies of data integration to derive quantitative information from the high-resolution images and investigate the effect of soil substrate (i.e., loam vs. sand) and the presence of root hairs on pH, phosphatase and labile P and Mn patterns. We started with radial parameter distribution extending from the root surface (rhizosphere gradients). Then, we defined spatial domains, *i.e.*, root surface, rhizosphere, and bulk soil, based on thresholds and calculated the average concentration/activity within these spatial domains. Furthermore, we investigated to which extent hotspots were associated with the rhizosphere and root surface, and to which extent the observed parameter hotspots were co-localized. To capture differences occurring along the roots, we compared young root tissues to older root regions.

2. Material and methods

2.1. Site description and experimental setup

All chemical imaging procedures were conducted at the experimental field site of the DFG priority program 2089 "Rhizosphere Spatiotemporal Organisation – A Key to Rhizosphere Functions" in Bad Lauchstädt, Germany (N 51.390424, E 11.875933). A detailed description of the experimental field site can be found in Vetterlein et al. (2021). Briefly, two maize genotypes (*Zea mays* L. wild-type (B73) (WT) and root hair defective mutant (*rth3*)) (Hochholdinger et al., 2008, 2018; Wen and Schnable, 1994) were grown on two substrates of different texture (loam L; and sand S; Table 1) in 6 replicate plots (each 3.1 × 11.0 m) in a randomized block design (Vetterlein et al., 2021). The treatments were L-WT, L-*rth3*, S-WT and S-*rth3*.The substrate 'loam' originated from the 0–50 cm depth of a Haplic Phaeozem near Schladebach, Germany (51°18′31.41″ N; 12°6′16.31″ E) which had been under agricultural use before excavation. The substrate 'sand' was obtained by sieving and mixing 16.7% of the beforementioned loam with

Table 1
General substrate characteristics before fertilization. Data are represent mean ± standard error ($n = 12$) (from Vetterlein et al. (2021).

Soil substrate	Loam	Sand	Method
Sand (%)	32.5 ± 0.36	91.8 ± 0.51	ISO 11277, 1998; ISO 11277, 2002
Silt (%)	47.9 ± 0.17	5.6 ± 0.35	
Clay (%)	19.5 ± 0.26	2.6 ± 0.17	
Bulk density (g cm^3)	1.39 ± 0.01	1.50 ± 0.01	
CEC ($mmol_c$ kg^{-1})	98.6 ± 4.7	33.1 ± 2.6	Ammonium acetate, pH 7 (Carter and Gregorich, 2007)
Soil pH ($CaCl_2$)	6.37	6.29	0.01 M $CaCl_2$ solution (soil:solution ratio of 1:2.5)
Organic C (g kg^{-1})	8.5 ± 0.1	1.5 ± 0.1	CNS analyzer
Total N (g kg^{-1})	0.83 ± 0.01	0.17 ± 0.01	CNS analyzer
Total P (mg kg^{-1})	416 ± 4.35	52.9 ± 4.68	Aqua regia (ISO 11466)
Iron oxides (g kg^{-1})	1.32 ± 0.01	0.25 ± 0.01	Oxalate + dithionate (Mehra and Jackson, 1960; Schwertmann, 1964)
P_{CAL} (mg kg^{-1})	32.7 ± 0.4	8.29 ± 0.37	Calcium acetate lactate (Schüller, 1969)
K_{CAL} (mg kg^{-1})	28.5 ± 0.72	7.84 ± 0.61	Calcium acetate lactate (Schüller, 1969)

83.3% quartz sand (WF 33, Quarzwerke Weferlingen, Germany). Both substrates were sieved < 4 mm and filled into the plots. General substrate characteristics before fertilization are shown in Table 1 and were already reported by Vetterlein et al. (2021). Both substrates were carbonate-free.

The amount of fertilizer applied to the field plots was experimentally pre-determined by Vetterlein et al. (2021) aiming at comparable nutrient availability for both substrates under homogenized (thorough mixing of substrate and fertilizer) and well-watered conditions. In the field, fertilizers were only surface applied and the substrates generally differ in water and nutrient transport, particularly under non-saturated conditions. To provide sufficient nutrients for maize growth while avoiding luxurious supply, soil plots were fertilized with nutrients at the rates (kg ha^{-1}) 50 N, 12 P, 50 K, 18 Mg, 27 Ca on loam, and 100 N, 24 P, 100 K, 33 Mg, 52 Ca + 100 Excello 331 Special (Jost GmbH, Micronutrients (%): 1 B; 3 Mn, 3 Zn, 0.3 Cu) on sand. The fertilizers included calcium ammonium nitrate, triple superphosphate, 60s corn potash and Epsom salt (Vetterlein et al., 2021). Fertilizers were surface applied in two rates: 50% prior to seeding and 50% at growth stage BBCH14 which corresponded to 14 and 6 weeks before the imaging campaign at growth stage BBCH 59, respectively. Planting density in the plots was 9.5 plants m^2 (Vetterlein et al., 2021), ensuring 2–5 plants per root window. Plant growth was characterized by cold spring, followed by a heat period with minimal precipitation that peaked during the imaging campaign. During the heat periods, prior to sampling, the soil area close to the root window was irrigated in the evening.

2.2. Root windows

Custom designed root windows were installed in 3 individual replicate plots per substrate and maize genotype combination, resulting in a total number of 12 root windows. Root windows were constructed on site in April 2019, prior to the first planting of the experimental plots. For root window installation, a pit (1 × 1 × 1.6 m) was excavated at the short end of each plot and three pit walls were stabilized by an open-end wooden crate inserted into the pit (Fig. 1a), which facilitates repeated access to the root windows during the entire duration of the SPP2089 program (6 years). Root windows were positioned at the open, top end of the crate. The wooden walls were stabilized with an aluminium bar (5 × 5 cm, Fig. 1b). The root windows were made from a grey PVC frame into which a transparent removable 5 mm thick acrylic glass plate with an observation area of 60 × 60 cm was inserted (Fig. 1c). The PVC window frame was inserted vertically (orthogonal to the soil surface) and fixed by a wooden stake construction, with the window frame reaching about 30 cm into the soil plots (Fig. 1a). Prior to the insertion of the removable observation plate, the entire observation area was covered by a transparent PVC plastic sheet (fixed onto the frame via tape) to protect the roots from damage when removing the observation plate. The PVC plastic sheet was renewed after every sampling event. The observation acrylic glass plate was then placed onto the soil and covered with two 30 × 60 cm grey PVC boards that were pressed against the soil block by two removable aluminium bars (3 × 3 cm) to provide stability and protection against light (Fig. 1b). The pressure of the PVC boards against the soil plot could be individually adjusted by wing bolts (Fig. 1b). In between the sampling events, the root window pits were covered with wooden boards (Fig. 1d). Fig. 1c shows a root window of one of the L-WT plots at BBCH 59.

2.3. Bio-chemical imaging

The imaging was conducted at the start of flowering (BBCH 59) (Bleiholder et al., 2001). Acid phosphatase activity was imaged with direct soil zymography, soil pH was visualized with planar optodes, and labile P and Mn-fluxes were imaged using diffusive gradients in thin films (DGT).

The three imaging techniques were consecutively applied within 2–3 days to all 12 root windows (3 replicates × 4 treatments, Table 2). Zymograms covered 10 × 20 cm (n_{total} = 19); pH optodes (2 x × 3 cm, n_{total} = 60) and DGT gels (1.5 × 2.5 cm, n_{total} = 41) were applied within the zymogram area at depth 10–50 cm with the focus on root tips and good soil-sensor/soil-gel contact while avoiding cavities. All sampling areas were sprayed with water before membrane/sensor/gel application to ensure good contact and diffusion while avoiding drying of sensors/gels and thus shrinkage. To avoid bias associated with diurnal plant processes, zymography membranes were always applied at the photosynthetic activity peak (10 a.m.–2 p.m.) for 1 h. For pH optodes, we used an optimized deployment time of ~12 h overnight to ensure a reliable pH signal under field moist conditions. DGT gels were deployed for 24 h to allow accumulation of labile nutrients over a complete day. The effect of changing weather and temperature conditions was randomized by sampling replicate windows over different days. The sequence of applied techniques within each window and the depth of application is presented in Table 2.

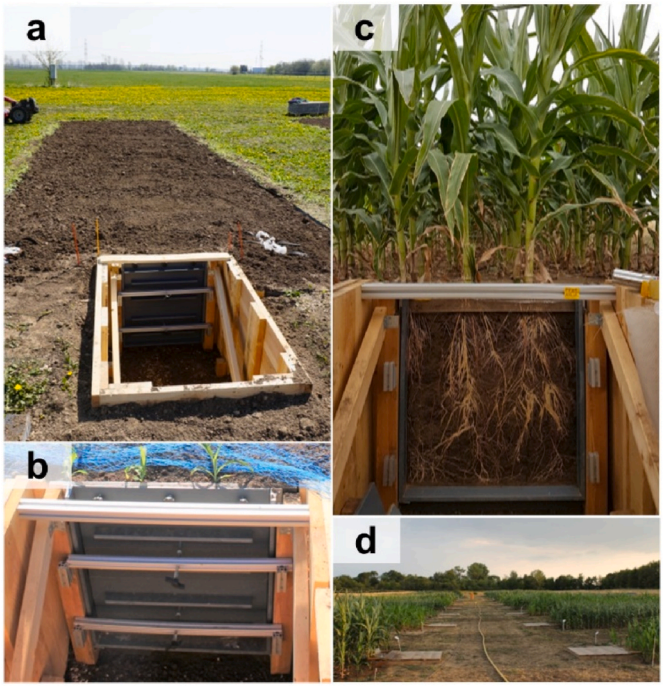

Fig. 1. Custom designed root window construction at the experimental field site of the DFG priority program 2089 "Rhizosphere Spatiotemporal Organisation – A Key to Rhizosphere Functions". (a) Experimental plot (loam) with newly installed root window construction and observation pit at the short end of the plot. (b) Close-up of the root window construction, with observation window being covered by two removable PVC boards that are pressed against the soil plot with aluminium bars and wing bolts for stability and protection against light. (c) Root window observation area (60 × 60 cm) of a loam plot planted with *Zea mays* L. wild-type (B73) at growth stage BBCH 59. (d) Root window pits covered by wooden boards in between sampling campaigns.

Acid phosphatase activity was detected by direct soil zymography as described in Razavi et al. (2019) with polyamide membranes soaked in 3.3 mM L^{-1} 4-methylumbelliferyl-phosphate disodium salt dissolved in MES buffer (pH 6.5) directly applied to the soil surface and covered with aluminum foil. A soft foam rubber was placed between the aluminum foil and acrylic glass plate to ensure optimal soil contact. After 1 h, the membranes were carefully lifted off and photographed in a dark room under ultraviolet light (excitation wavelength 355 nm). Calibration was performed as described in Razavi et al. (2019). Zymograms were transformed to 8-bit grayscale images in ImageJ (Schindelin et al., 2012) and calibrated to acid phosphatase activity (Section S1, Eq. S(1)).

Planar optodes (sensor foils SF-HP5R) combined with the VisiSens TD imaging system from PreSens GmbH (Regensburg, Germany) were

Table 2
Application sequence of imaging techniques including number of zymograms, optodes and DGT gels applied, number of regions of interest (ROI) used for image analysis with corresponding position (distance from the soil surface) within the root window. Biological replicates are represented by the root system grown in individual root window from different field plots Note that analysed DGT replicates were limited due to application challanges in the field (cavities, poor contact).

Fieldplot (biological replicate)	Substrate	Genotype	Method sequence	Days between first and last assay	Number of zymograms applied	Number of optodes applied	Number of DGT gels applied	ROI for analysis pH & zymo.	ROI for analysis DGT	Position in window (distance from soil surface)
FP01	Loam	Wildtype	DGT-zymo-optode	1	1	5	3	1		40–50 cm
FP02	Loam	Wildtype	DGT-zymo-optode	1	1	4	2	2	1	10–20 cm
FP03	Loam	Wildtype	DGT-zymo-optode	1	1	6	3	3	2	20–40 cm
FP07	Loam	*rth3*	DGT-zymo-optode	1	3	7	5	2	1	20–30 cm
FP08	Loam	*rth3*	DGT-zymo-optode	1	2	3	3	1	1	20–30 cm
FP09	Loam	*rth3*	DGT-zymo-optode	1	2	6	4	2	1	30–40 cm
FP13	Sand	Wildtype	Optode-zymo-DGT	2	2	4	4	1		40–50 cm
FP14	Sand	Wildtype	Zymo-DGT-optode	3	1	5	3	1		10–20 cm
FP15	Sand	Wildtype	Zymo-DGT-optode	2	1	7	3	3	2	30–40 cm
FP19	Sand	*rth3*	Optode-zymo-DGT	2	2	3	5	1		30–40 cm
FP20	Sand	*rth3*	Zymo-DGT-optode	3	1	7	3	2	1	30–40 cm
FP21	Sand	*rth3*	Optode-zymo-DGT	2	2	3	3	2	1	30–40 cm
Total					19	60	41	21	10	

used to visualize pH (Blossfeld and Gansert, 2007). The self-adhesive sensor foils were cut and pasted on a transparent polyester foil (125 μm thick, Melinex®506, DuPont Teijin Films, USA), pre-equilibrated in phosphate-NaCl buffer (pH 6.5, ionic strength 100 mM) and then fixed on the inner side of the root window observation plate with tape. Sensor foils were applied overnight (~12 h), and images were recorded in the morning in dark conditions using black cloth to cover the observation pits. The camera was placed directly on the observation plate to keep a constant distance between camera and optode resulting in a field of view of 5 cm × 3.7 cm. The ionic strength of the soil solution was estimated from the electrical conductivity as described in SI (Section S2). Sensor foils were calibrated using phosphate buffers (pH 5.0 to pH 8.5) with the ionic strength adjusted with NaCl to 40 and 16 mM for loam and sand, respectively. The details are described in Section S2 in SI.

DGT solute binding gels were applied to map labile nutrient fluxes. By exposing an infinite solute sink to soil, DGT continuously accumulates the targeted solute species, here P and Mn. The accumulated solute mass is often reported as time-averaged solute flux (pg cm^{-2} s^{-1}) from the soil to the gel, which provides a measure of the local solute resupply capacity of the soil. In the DGT imaging setup, this allows for a relative comparison between different locations. The DGT gels were prepared as described by Kreuzeder et al. (2013) (for details see also Supplementary Information – Section S3). Gels were covered by a Nuclepore membrane (Nuclepore Track-Etched Membrane 0.2 μm, Whatman, UK) and fixed to acid washed Melinex foil and mounted to the inner side of the root window observation plate. Two layers of sponge cloth pieces were fixed between the observation plate and the grey PVC stabilization boards at the position of each DGT gel to improve the soil-gel contact when closing the window. After 24 h, the gels were retrieved, rinsed with deionised water, and dried. Spatial distribution of elements captured by the DGT was analysed by laser-ablation inductively coupled mass spectrometry (LA-ICPMS). LA-ICPMS was performed in line scanning mode (interline distance 400 μm, spot size 150 μm, laser speed 150 μm s^{-1}) with a UP 193-FX (ESI, NWR Division, Portland, USA) laser ablation system coupled to a quadrupole ICPMS (Elan 9000 DRCe, PerkinElmer, Waltham, MA, USA). The resulting pixel size in the images was 99.4 μm × 400 μm. Details regarding gel analysis and calibration are described in the supporting information (Section S3) and in Wagner et al. (2020). Depending on the DGT-soil-root-interface contact, two to three DGT replicate images per treatment were analysed (Table 2).

2.4. Image analysis

Image analysis of pH and acid phosphatase activity was based on 5–6 regions of interest (ROI) per treatment (Table 2), not necessarily representing 3 biological replicates as the quality of some ROI was not optimal due to poor contact or large cavities. For DGT less ROI were available (3 in L-WT, 3 in L-*rth3*, 2 in S-WT and 2 in S-*rth3*) due to the challenging field conditions (cavities, contact issues) and generally lower number of DGT-gels ($n_{total} = 41$).

Root photographs and DGT images were scaled to the size of pH maps and zymograms (resolution 0.038 mm per pixel) without interpolation in ImageJ Fiji (Schindelin et al., 2012). The images were aligned in Photoshop (CS5, V12.0) with the help of photographs during the application. It must be noted that the angle of some root photographs was not perfectly orthogonal resulting in small image distortions and

slight inaccuracies in scaling and rectification. Templates (*e.g.,* angle for rotation and coordinates for alignment) prepared in Photoshop were used for extracting the ROI for analysis in ImageJ. Root masks were prepared from the root photographs in ImageJ by drawing lines along the roots and adjusting the line thickness to each individual root. Rhizosphere extent was determined with plots of average concentration in soil as a function of root distance, *i.e.*, concentration-distance plots (Fig. S1, step 2). These were computed according to Lucas et al. (2019) with adaptations for 2D images. Briefly, a "Euclidian Distance Transform" (EDT) function was applied on the binary root mask image with the "Exact Euclidian Distance Transform (3D)" method in ImageJ resulting in a distance map, where a grey value corresponding to the distance to the closest root was assigned to each pixel. The distance map was then combined with the analyte image (phosphatase, pH images, or DGT flux; further transformed to 8-bit grayscale, according to minimum and maximum value) into a composite image. Every pixel in the composite image contained the concentration in one channel and the distance to the closest root information in another channel. A loop in the x and y dimensions was then initiated on the composite image to retrieve the information of both channels simultaneously. The average analyte concentration for each distance class (class width 0.038 mm) from the root, was saved as text file. More information and the ImageJ script can be found in Lucas et al. (2019). In addition to distance classes, we defined 3 spatial domains in each analyte image: bulk, rhizosphere, and root surface (Fig. S1). Bulk soil concentrations were measured in the image area remaining after subtraction of the root mask enlarged by 2.5 mm. Root surface concentration was measured on the area of the root mask. Note that the spatial domain 'root surface' refers to root surface exposed, *i.e.*, in direct contact with the measurement device (membrane, optode, DGT gel) without soil in between and hence reflects activity of the root.

The gradual rhizosphere extent in the concentration-distance plots was compartmentalized with activity/concentration thresholds to define an artificial boundary between rhizosphere and bulk soil and hence to calculate 'the average rhizosphere extent' (individual rhizosphere for each investigated parameter): for each ROI image, an individual threshold was calculated by adding two times the respective standard deviation ($+2 \times$ SD; or $-2 \times$ SD in the case of pH) to the determined average bulk soil concentrations/activities (Fig. S1). Note that an individual threshold for each ROI was also required to cope with variations in bulk concentrations/activities due to differences in moisture content during sampling campaign (sunshine vs. rain). These thresholds were also used to (i) define hotspots (*i.e.*, all activities/concentrations greater (or lower in case of pH) than the determined threshold) (ii) determine the relative spatial hotspot coverage (% of total area) of each spatial domain and (iii) to create binary hotspot images for co-localization analysis. Analysis of spatial co-localization/coincidence of hotspots for four parameters (acid phosphatase activity, pH (acidification), Mn and P-fluxes) was performed using 'Just another co-localization plug-in' (JACoP) (Bolte and Cordelières, 2006) in ImageJ. The thresholded binary images of hotspot activities for each parameter were created for two spatial domains (root surface defined by root masks and standardized rhizosphere of 2.5 mm to ensure the same co-localization areas) separately and corresponding co-localization analysis was done, *i.e.*, how much area of one parameter co-localizes with the area of another parameter. The calculated overlap coefficient (r, Eq. (1)) represents the percentage of the overlapping hotspot areas from two parameters (A, B) and shows the share of common hotspot area of the two parameters within the cumulative hotspot area of the same two parameters:

$$\text{Overlap coefficient } (\%)\ r = \frac{\sum_i A_i \cdot B_i}{\sqrt{\sum_i A_i^2 \cdot \sum_i B_i^2}} * 100 \quad (1)$$

Where A_i – is the value at each pixel of image A, B_i – is the value at each pixel of image B.

Spatial changes along the root axis were assessed by measuring root surface pH, acid phosphatase activity, P and Mn-flux for young root tissues (<2 cm from root cap) and older root sections (>4 cm from root cap).

2.5. Statistics

All data are presented as mean ± standard error (SE) of 5–6 replicate ROIs for zymograms and optodes deriving from 3 root windows and 2–3 replicates for DGT ROIs deriving from 2, 3, 1, and 2 root windows for L-WT, L-*rth3*, S-WT and S-*rth3*, respectively (Table 2). The Shapiro-Wilk test was performed for residues of means to check for normality, and the Bartlett test was applied to check the homogeneity of variances. All data were log transformed for statistical analysis. T-test, one- or two-way ANOVA and Tukey's HSD post-hoc test were performed in RStudio (version March 1, 1093) at a significance level of $\alpha = 0.05$. Figures were prepared in Sigma Plot (V.12.0, Systat Software Inc.) and Microsoft Publisher for Microsoft 365 (V2010).

3. Results

Generally, both maize genotypes grew better on loam (L) than on sand (S), and the wildtype (WT) developed a higher shoot biomass than the root-hair defective mutant (*rth3*) irrespective of substrate (see also Vetterlein et al., 2021). At BBCH 59, P contents (mg plant^{-1}) were highest in L-WT (180 ± 25) followed by L-*rth3* (105 ± 6), S-WT (71 ± 5) and S-*rth3* (58 ± 6) (Vetterlein et al., in preparation).

3.1. Direct observations on high resolution images

Acidification features were observed mainly on/around root tips and actively growing roots (Figs. 2 and S2). Elevated acid phosphatase activity was relatively homogenously distributed along the roots in all treatments (Figs. 2 and S3 and b). P depletion zones were not clearly pronounced, patchy and only inconsistently observed around some older root sections (Fig. 2, white arrows). Increased P and Mn fluxes occurred mainly on the root surface at the root tips (Fig. 2, red arrows, and Fig. S4).

3.2. Rhizosphere gradients and boundaries between spatial domains (i.e., average rhizosphere extents)

Generally, rhizosphere gradients were either comparable or steeper in sand than in loam. Average rhizosphere extents were greater in sand when compared to loam (Fig. 3). However due to the large image heterogeneity, most of the observed differences in rhizosphere extents were not statistically significant, except for phosphatase activity, where we found a significant effect of substrate (Fig. 3 & Table S1). The rhizosphere extent for acidification tended to increase in the order L-WT (mean ± SE: 0.79 ± 0.42 mm) < L-*rth3* (0.98 ± 0.48 mm) < S-WT (1.25 ± 0.34 mm) < S-*rth3* (1.45 ± 0.40 mm) (Fig. 3). Acid phosphatase activity rhizosphere extents were significantly larger in sand (S-WT: 1.59 ± 0.36 mm; S-*rth3*: 1.26 ± 0.24 mm) than in loam (L-*rth3*: 0.62 ± 0.45 mm; L-WT 0.29 ± 0.16 mm; $p=0.005$, Table S1), with no significant difference between genotypes. The average rhizosphere gradients of P fluxes showed no clear trend, and no rhizosphere extents could be defined from the concentration-distance plots (Fig. 3). The rhizosphere gradients of Mn flux showed a slightly steeper decrease in *rth3* than in WT in both substrates combined with less pronounced rhizosphere extents for *rth3* (0.27 ± 0.14 and 0.75 ± 0.21 mm in L and S, respectively) than for WT (0.88 ± 0.47 and 1.12 ± 0.04 mm in L and S, respectively) ($p=0.160$, Table S1, Fig. 3).

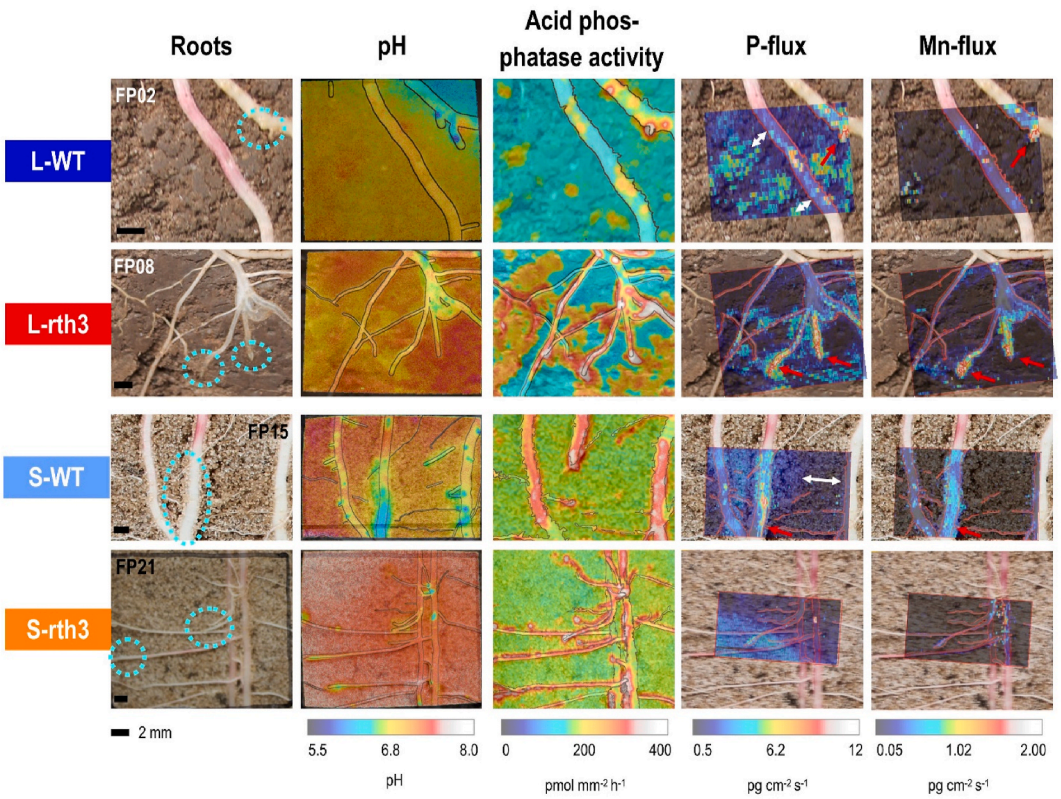

Fig. 2. Exemplary root images, pH, acid phosphatase activity (pmol mm^{-2} h^{-1}), P flux and Mn flux (pg cm^{-2} s^{-1}) images (overlaid on the corresponding root image with 50% transparency) of two maize genotypes (wild-type (WT) and root hair defective mutant (*rth3*)) grown in root windows on loam (L) and sand (S) in the field. The identification number of each field plot (FP) is indicated in the top part of root images. Dotted circles highlight actively growing roots during method application. Red arrows highlight P hotspots at actively growing root tips and white arrows indicate possible P depletion zones around older roots. (For interpretation of the references to color in this figure legend, the reader is referred to the Web version of this article.)

3.3. *Average pH, acid phosphatase activity, P and Mn fluxes in individual spatial domains (bulk soil, rhizosphere and on root surface)*

Despite the patchiness of visualized parameter values (Fig. 2), averaging activities/concentration/fluxes within each spatially defined domain (root surface, rhizosphere, bulk soil) showed distinct trends (Figs. 3 and 4). Acidification was found on the young root tissue surface of both maize genotypes that extended into the adjacent rhizosphere (Fig. 4a). For *rth3* the decrease in averaged pH from the bulk soil > rhizosphere > root surface was statistically significant irrespective of growth substrate (Fig. 4a). The same trend was observed for WT; however, the differences were not statistically significant. Bulk pH was 7.06 ± 0.06 and 7.30 ± 0.06 in loam and sand, respectively. As expected, rhizosphere acidification was on average more pronounced in sand (by 0.21 ± 0.03 pH units) than in loam (by 0.12 ± 0.02 pH units). Average root surface pH was 6.80 ± 0.13, 7.01 ± 0.12, 6.89 ± 0.30 and 6.94 ± 0.23 in L-WT, L-*rth3*, S-WT and S-*rth3*, respectively and did not differ between the treatments.

Average acid phosphatase activity tended to increase across spatial domains in the order bulk - rhizosphere – root surface with more distinct differences in sand than in loam (Fig. 4b). However, neither a statistically significant genotype nor a substrate-specific effect in any of these spatial domains (p=*0.216-0.887*, Table S2) were observed. Irrespective of genotype and substrate, phosphatase activity was 36 ± 0.03% higher on the root surface and 11 ± 0.10% higher in the rhizosphere than in the bulk soil.

Average P flux (representing a measure of the local solute resupply capacity of the soil s triggered by biogeochemical conditions) for S-WT showed on average a higher P flux on the root surface compared to rhizosphere and bulk soil while it remained constant among the spatial domains for other treatments (Fig. 4c). The elevated P flux in S-WT was mainly associated with thick root tips that were actively growing during DGT application and extended slightly into the rhizosphere.

Averaged Mn flux increased in the order bulk – rhizosphere – root surface irrespective of substrate and genotype. Due to the heterogeneity within and between the replicate images (see above), observed differences were mainly non-significant, except for S-WT which displayed a significant higher average Mn flux on the root surface compared to bulk soil (Fig. 4d).

3.4. *Root surface and rhizosphere hotspot distribution*

Calculating the relative coverage of areas identified as activity hotspots (defined as bulk soil activity/concentration + 2 x SD for phosphatase activity, P, Mn flux; - 2 x SD for pH) revealed a rather patchy hotspot distribution that differed for each investigated parameter. Relative hotspot coverage on root surface and in the rhizosphere was greatest for acidification (73 ± 4 and 63 ± 2%) followed by phosphatase activity (70 ± 4 and 49 ± 3%), Mn flux (59 ± 8 and 42 ± 4%) and P flux (24 ± 5 and 22 ± 5%) of root surface and rhizosphere area, respectively, averaged across all substrates and genotypes, with generally greater hotspot coverage on the root surface than in the rhizosphere and a mostly non-significant trend of greater hotspot coverage in sand than in loam (Fig. 5, Table S3). Bulk soil hotspot coverage was 35 ± 2%, 15 ± 2%, 22 ± 3%, and 18 ± 2% for pH, phosphatase activity, P and Mn flux, respectively (Fig. 5). Differences between root surface and rhizosphere were only statistically significant in sand for pH (*rth3* only) and Mn-flux (WT only, Fig. 5, Table S4). The hotspot coverage for root surface pH and acid phosphatase activity was significantly higher in sand than in loam (p=*0.04* and p=*0.03*, respectively, Table S3), but there was no

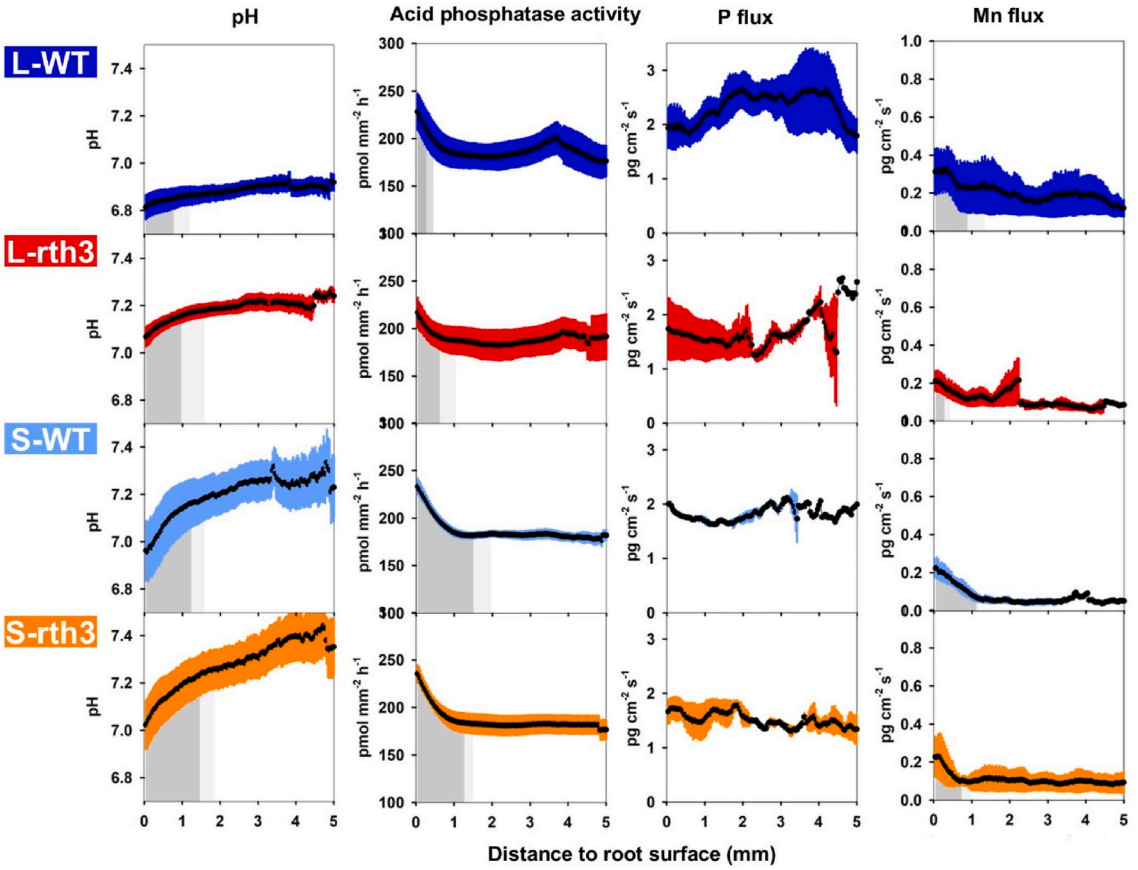

Fig. 3. Average pH, acid phosphatase activity, P and Mn flux as a function of distance to the root surface of two maize genotypes (wild-type (WT) and root hair defective mutant (*rth3*)) grown in loam (L) and sand (S). Coloured error bars represent standard error of $n = 6$ (L-WT) or $n = 5$ (L-*rth3*, S-WT, S-*rth3*) for pH and acid phosphatase activity; $n = 3$ (L-WT, L-*rth3*) or $n = 2$ (S-WT, S-*rth3*) for P and Mn flux. The average rhizosphere extent is shown as dark grey areas and was determined from individual concentration-distance plots with a threshold value (mean concentration at distance >2.5 mm (*i.e.*, bulk soil ± 2xSD); light grey areas indicate standard error for the average rhizosphere extent. No rhizosphere extent was defined for P flux.

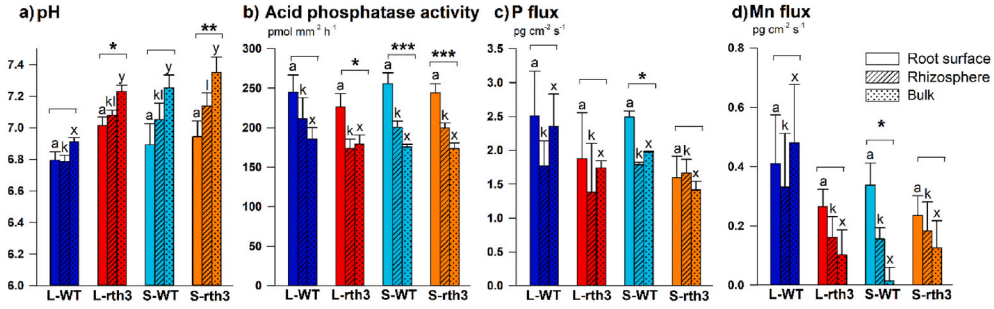

Fig. 4. Averaged **(a)** pH, **(b)** acid phosphatase activity, **(c)** P and **(d)** Mn fluxes of bulk soil (area excluding root surface mask enlarged by 2.5 mm), rhizosphere (individual rhizosphere extent) and root surface (area of image covered by root tissue only) of two maize genotypes (wild-type (WT) and root-hair defective mutant (*rth3*)) grown in loam (L) and sand (S). Error bars represent SE of n = 6 (L-WT), or n = 5 (L-*rth3*, S-WT, S-*rth3*) for pH and acid phosphatase; n = 3 (L-WT, L-*rth3*) or n = 2 (S-WT, S-*rth3*) for P and Mn flux. *Note: P rhizosphere flux was measured within the area of Mn rhizosphere extent, as no P rhizosphere extent could be defined.* Letters above the bars indicate significant differences between treatments according to two-way ANOVA for each spatial domain according to Tukey post-hoc test, *i.e.,* root surface (a), rhizosphere (k–m), and bulk (x–y). Asterisks indicate significant differences between the spatial domains (bulk, rhizosphere, root surface) within one treatment (one-way ANOVA, '.' $p < 0.10$, '*' $p < 0.05$, '**' $p < 0.01$, '***' $p < 0.001$).

statistically significant effect of genotype for any of the parameters (Table S3).

3.5. Co-localization of hotspots

Spatial co-occurrence of parameter hotspots indicates possible interactions of P solubilizing processes. Overlap coefficients show the share of the common hotspot area of two parameters within the cumulative hotspot area of the same two parameters. Acidification and acid phosphatase hotspots showed a high co-localization on the root surface as revealed by relatively high overlap coefficients (*i.e.*, L-WT 63 ± 3%, L-*rth3* 66 ± 9%, S-WT 79 ± 4%, S-*rth3* 81 ± 7%), with a pronounced

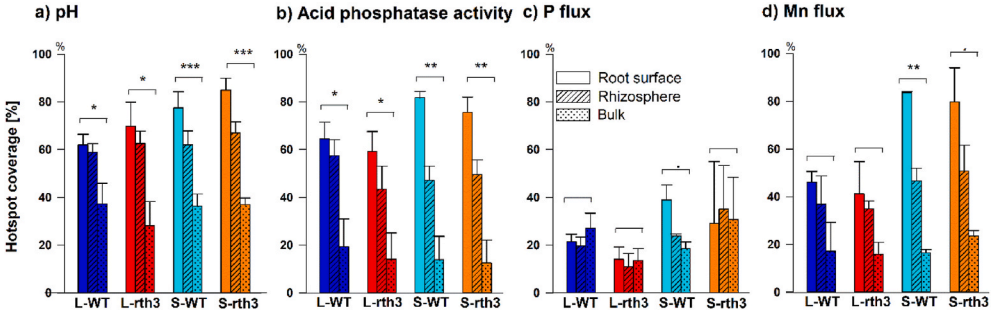

Fig. 5. Hotspot coverage of pH (a), acid phosphatase activity (b), P flux (c), and Mn flux (d) on the root surface, in the individual rhizosphere and in the bulk soil expressed as relative percentage based on the total area of respective spatial domain. Bars and error bars represent mean and standard error of L-WT (n = 6), L-*rth3* (n = 5), S-WT (n = 5), S-*rth3* (n = 5) for pH and phosphatase, for P and Mn flux, L-WT and L-*rth3* (n = 3); and S-WT and S-*rth3* (n = 2). Note that P rhizosphere flux was measured in the Mn rhizosphere. Asterisks indicate significant differences between root surface, rhizosphere, bulk hotspot coverage according to one way-ANOVA (' ' n.s., '.' $p < 0.10$, '*' $p < 0.05$, '**' $p < 0.01$).

substrate (p=*0.028*) but no genotype (p=*0.969*) effect (Table 3). Co-localization of Mn-flux hotspots with hotspot phosphatase activity (70 ± 5%, averaged across all treatments) and acidification (67 ± 6%) on the root surface was in a similar range as co-localization of hotspot phosphatase activity and acidification (72 ± 3%) (Table 3). In line with the relative area covered by individual parameter hotspots (Fig. 5), overlap coefficients for pH-phosphatase, pH-Mn and phosphatase-Mn were smaller in the rhizosphere compared to the root surface and generally followed a similar though less distinct trend as observed for the root surface (Table 3). Low overlap coefficients of P flux hotspots with acidification or acid phosphatase hotspots (35 ± 4% to 40 ± 5%) on root surface were mainly determined by the much lower occurrence of P flux hotspots in comparison to acidification and phosphatase hotspots (Fig. 5). P-related overlap coefficients (pH-P, phosphatase-P and Mn–P) also only showed minor, mostly non-significant differences between the root surface and the rhizosphere (Table S5).

3.6. Spatial dynamics along the root axis

While average parameters within each spatial domain are useful to report general trends of soil texture and genotypes, the high variability within and between replicates mostly only showed non-significant differences. Thus, we conducted a more spatially resolved analysis to identify differences occurring along the root in axial direction and to unravel potential treatment effects. Younger root tissues (<2 cm from root cap) were 0.35–0.68 pH units more acidic than older root tissues (>4 cm from root cap) with wild-type root tips being generally more acidic than tips of root-hair defective mutant (*rth3*), irrespective of the substrate (Fig. 6, Table S6). pH values on the older root sections were not significantly different from bulk soil pH (Table S6). Acid phosphatase was slightly higher at younger root tissue than at older ones, but no genotype or substrate effect could be observed. For P and Mn flux at young and older root tissue no significant trend was observed due to the large variability between roots.

4. Discussion

4.1. Methodological challenges

For the first time, planar optodes, zymography, and DGT were successfully combined under field conditions to visualize pH, acid phosphatase activity and labile P and Mn around roots of older maize plants (growth stage BBCH 59) grown in a real agroecosystem environment with uncontrolled weather conditions, which would not have been possible in the laboratory. However, working in the field, the following conditions challenged image analysis which need to be considered when interpreting our findings: i) root tips were growing during and between the method applications (total duration for individual root window: 2–3 days), which made image overlay and co-localization analysis more difficult; ii) contact between probes and soil/root was not always perfect and more difficult to control compared to lab conditions; iii) especially in loam, large pores between big aggregates inhibited diffusion and contributed to a high degree of variability; iv) high root density, overlapping rhizospheres combined with generally small regions of interest (especially for DGT) limited the root-free areas on the analysed images and the number of replicates of comparable root types and sections; v) areas obviously affected by artefacts needed to be excluded from analysis reducing the number of actually analysed replicates (for details see Table 2); vi) due to the dense root systems and the presence of 2–5 plants per root window, we were not able to identify different root types, *e.g.* embryonal primary and seminal roots, shoot-borne crown roots, and laterals of several orders, which all possess different functions in terms of nutrient and water acquisition, transport, anchorage (Hochholdinger et al., 2004); vii) aligning of images with different resolution is prone to error due to small inaccuracies in scaling and rectification, if the angle of root photographs was not perfectly orthogonal. Despite these difficulties, we investigated general trends of root surface and rhizosphere pH, phosphatase activity and labile P and Mn driven by soil substrate and the presence of root hairs by averaging over different root types and positions along the root with different root diameters (*i.e.*, cap, elongation zone, root-hair zone, mature parts) and across as many technical replicates as possible.

In addition to the challenge of actively growing roots during our chemical imaging campaign, the consecutive application of different imaging techniques could potentially introduce a bias in our results as one imaging technique could affect the results of the following one. However, we observed the same general trends in our images from both substrates, even though the image technique application sequence differed between both substrates (Table 2). Consequently, we rule out any significant influence of the previously applied imaging technique to the results of the following one. Furthermore, maximum P input after zymography application can be expected to be around 0.003 ng cm^{-2} (maximum potential mass accumulation on a DGT that can be derived from a soaked membrane after 1 h membrane application with a 10 × 20cm membrane soaked in 5 mL 3.3 mM MUF-P), which is negligible compared to the bulk soil DGT-P accumulation in our soils >100 ng cm^{-2} (mass accumulation on a DGT sampler after 24 h application period, corresponds to a P flux >1.16 pg cm^{-2} s^{-1}, Figs. 3 and 4). Although pH optodes were pre-equilibrated in 20 mM L^{-1} phosphate buffer, the optode matrix does not chemically interact with P and optodes were carefully rinsed before application (see more details below), consequently rendering it unlikely to affect detected P fluxes.

4.2. Acidification

We attribute the steeper rhizosphere gradients of pH in sand compared to loam irrespective of genotype (Fig. 3) to the higher pH buffer capacity of loam due to the greater presence of secondary minerals, clay, and organic matter (Table 1). Moreover, the effective diffusion coefficient of protons is larger in sand compared to loam (Olesen

Table 3

Top: Overlap coefficients for co-localized hotspots of acidification (pH), acid phosphatase, P and Mn flux in two spatial domains (root surface and rhizosphere) across treatments. Data represent means ± SE, following by the number of replicates for pairs of parameters in parentheses (n). **Bottom:** *p-values* from two-way ANOVA comparing the effect of substrate, genotype, and their interaction across treatments within each parameter combination. Significant effects ($p < 0.05$) are marked **in bold.** Different letters in each column indicate significant ($p < 0.05$) difference between treatments within each parameter combination as revealed by the corresponding Tukey post-hoc test.

Treat ment	Overlap coefficient for co-localized hotspots, %										
	pH-phosphatase (a,b)	pH-P (c,d)	pH-Mn (e,f)	Phosphatase-P (g,h)	Phosphatase-Mn (k,l)	P–Mn (m,n)	pH-phosphatase (a,b)	pH-P (c,d)	pH-Mn (e,f)	Phosphatase-P (g,h)	Phosphatase-Mn (k,l)	P–Mn (m,n)
	Root surface						Standardized rhizosphere (2.5 mm)					
L_WT	64 ± 3^{a} (n = 6)	32 ± 4^{c} (n = 3)	52 ± 4^{c} (n = 3)	44 ± 5^{g} (n = 3)	62 ± 6^{k} (n = 3)	53 ±4^{m} (n = 3)	42 ±6^{a} (n = 6)	28 ±7^{c} (n = 3)	31 ± 10^{e} (n = 3)	36 ± 2^{g} (n = 3)	39 ± 11^{k} (n = 3)	34 ± 9^{m} (n = 3)
L_*rth3*	66 ± 9^{a} (n = 5)	34 ± 8^{c} (n = 3)	58 ± 11^{e} (n = 3)	33 ± 8^{g} (n = 3)	57 ± 10^{k} (n = 3)	44 ±9^{m} (n = 3)	41 ± 10^{a} (n = 5)	31 ± 4^{c} (n = 3)	35 ± 6^{e} (n = 3)	33 ± 4^{g} (n = 3)	33 ±3^{k} (n = 3)	38 ±0^{m} (n = 3)
S_WT	79 ± 4^{a} (n = 5)	39 ± 1^{c} (n = 2)	82 ± 6^{e} (n = 2)	40 ± 11^{g} (n = 2)	86 ± 3^{k} (n = 2)	48 ±5^{m} (n = 2)	53 ±2^{a} (n = 5)	38 ± 0^{c} (n = 2)	59 ±2^{e} (n = 2)	31 ± 3^{g} (n = 2)	56 ± 2^{k} (n = 2)	50 ±4^{m} (n = 2)
S_*rth3*	81 ± 7^{a} (n = 5)	37 ± 20^{c} (n = 2)	82 ± 10^{e} (n = 2)	42 ± 27^{g} (n = 2)	87 ±3^{k} (n = 2)	40 ± 22^{m} (n = 2)	52 ±5^{a} (n = 5)	36 ± 10^{c} (n = 2)	45 ± 2^{e} (n = 2)	42 ± 20^{g} (n = 2)	46 ± 4^{k} (n = 2)	51 ± 3^{m} (n = 2)
Overall mean	**72 ± 3 (n=21)**	**35 ± 4 (n=10)**	**67 ± 6 (n=10)**	**40 ± 5 (n=10)**	**70 ± 5 (n=10)**	**47 ± 5 (n=10)**	**47 ± 3 (n=21)**	**32 ± 3 (n=10)**	**41 ± 5 (n=10)**	**35 ± 3 (n=10)**	**42 ± 4 (n=10)**	**42 ± 3 (n=10)**
Two-way ANOVA												
Substrate	***0.0277****	*0.780*	***0.0234****	*0.929*	***0.0386****	*0.584*	***0.0276****	*0.331*	*0.136*	*0.994*	***0.0805***	***0.0586***
Genotype	*0.9686*	*0.809*	*0.6630*	*0.458*	*0.6751*	*0.331*	*0.7926*	*0.851*	*0.883*	*0.950*	*0.4839*	*0.5176*
Substrate Genotype*	*0.9129*	*0.722*	*0.8779*	*0.817*	*0.7084*	*0.817*	*0.9851*	*0.636*	*0.420*	*0.574*	*0.8253*	*0.6363*

et al., 2001) contributing to ~0.45 mm larger rhizosphere extents in sand (on average 1.35 mm) than in loam (on average 0.89 mm, Fig. 3). Similar rhizosphere extents were also found for younger maize crown roots by Rudolph-Mohr et al. (2017), who observed acidification up to 1 pH unit within 0.75–1.5 mm from the root surface in a sandy soil.

Rhizosphere acidification under P limiting conditions has often been associated with the release of organic acids. However, organic acids only marginally contribute (0.2–0.3%) to acidification by maize roots as they are exuded as deprotonated acid anions due to their low p*Ka* and a cytosolic pH of around 7 (Hinsinger, 2001; Jones, 1998; Petersen and Böttger, 1991). Also, the release of protons to maintain the charge balance upon NH_4^+ uptake was often linked to rhizosphere acidification (Hinsinger et al., 2003; Prjanischnikow, 1929; Sorrell and Orr, 1993). In our case, extrusion of protons by maize roots according to the acid growth theory seems more likely, as acidification occurred mainly around root tips and young root tissue which actively grew during optode application (~12 h) (Fig. S2). According to the acid growth theory, the extrusion of protons from the cytosol through plasma membrane into the apoplast supports the loosening of the cell wall stimulating cell expansion (Hager, 2003). At the end of cell growth the calcium ion concentration in the cytosol is increased which inhibits the H + -ATPase activity raising the apoplastic pH consequently halting wall expansion. (Majda and Robert, 2018). The pH measured on the surface of young root tissue of the wild-type was 0.3–0.4 pH units more acidic than that of young root parts of the root-hair defective mutant (*rth3*)also supports that root tissue growth coincides with rhizosphere acidification as our observations can be linked to the growth of root hairs. Furthermore, the observed increased in labile calcium concentration in the DGT images of growing root tissues (Fig. S5) would suggest that some of this Ca is released from the cytosol during this signalling cascade.

4.3. Root and microbially-derived acid phosphatase activity

Similar to pH, acid phosphatase activity rhizosphere extents were larger in sand than in loam, but neither average root surface nor average rhizosphere acid phosphatase activity differed significantly between the genotypes or substrates (Fig. 4b). As enzyme diffusion in soil is negligible (Guber et al., 2018), we attribute the larger rhizosphere extent to a greater activity of phosphatase-releasing microbes in the rhizosphere of sand-grown maize. Maize derived root exudates (*i.e.*, C-containing primary and secondary metabolites released by roots) (Bilyera et al., 2021, Santageli et al., in prep) can be expected to be more strongly sorbed in loam than in sand hence limiting exudate diffusion and consequently the extent of their microbial stimulation effect in loam. Moreover, sorption of extracellular enzymes to soil minerals can protect them from degradation and change their biochemical properties and thus their activity and persistence in soil. The specific activity of enzymes was found to be higher after sorption to a soil with a low sorption site availability, such as the sand in our study, compared to soils with more abundant sorption sites, *i.e.*, the loam (Olagoke et al., 2019, 2020), which possibly also explains the larger rhizosphere extent in sand.

In contrast to other studies investigating different species, we did not find a significant effect of root hairs on phosphatase activity and its related rhizosphere extent. Root hairs of this maize genotype were with only ~0.24 mm (Lippold et al., 2021) rather short compared to other species such as barley, which could explain why we did not observe a clear genotype effect on the rhizosphere extents. Nevertheless, similar acid phosphatase rhizosphere extents of around 1 mm were found by Kandeler et al. (2002) after soil slicing (resolution 0.2 mm) or by Ma et al. (2018) (1–2 mm measured with zymography from the root centre) and Razavi et al. (2016) for younger maize plants (7–21 days old). Nevertheless, our results are comparable to these zymography studies when adding the root radii (ranging from 0.1 to 1.0 mm) to the rhizosphere extents.

Efficacy of phosphatases generally depends on P_o availability and P esters might strongly sorb to the soil solid-phase (Huang et al., 2005),

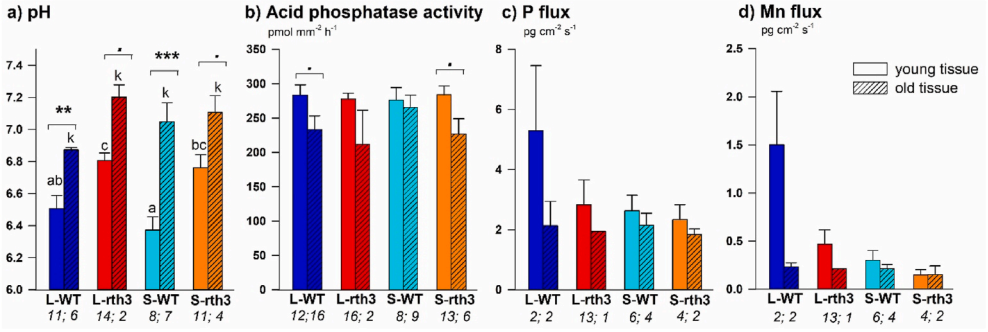

Fig. 6. Spatial differences along root axis: Root surface pH (a), and acid phosphatase activity (b), P (c) and Mn flux (d) of young (<2 cm from root cap) and older root tissue (>4 cm from root cap). Number below each bar represents replicates (individual root sections on which the parameter was measured). Asterisks indicate significant differences between young and older tissues (*t-test* with '.' $p < 0.10$, '*' $p < 0.05$, '**' $p < 0.01$). Letters indicate significant differences between the treatments for young tissues (a–c) and old tissues (k) (two-way ANOVA $p < 0.05$, Tukey post-hoc test).

which limits hydrolysis by phosphatases (Gerke, 2015). In loam, P_o (estimated from soil organic matter, Section S4) was nearly 6-times higher compared to sand. Hence, in loam similar phosphatase activities in the rhizosphere could have mobilized a larger amount of phosphate from P_o compared to sand.

In contrast to the rather homogenous distribution of phosphatase activity along the entire root for barley (Holz et al., 2020), we found a trend of higher phosphatase activity on young compared to older root sections which was significant ($p < 0.01$) for L-WT and S-rth3 (Fig. 6, Table S6). Holz et al. (2020) found that 4-week-old root-hairless barley had higher phosphatase activity than the wild-type barley which developed larger acid phosphatase rhizosphere extents in the root hair zone than the mutant. Contrastingly, in this study the influence of root hairs on acid phosphatase activity was negligible for 12-week-old maize (Fig. 4b).

4.4. P flux

DGT images provide a snapshot of labile nutrient patterns on the root and in the rhizosphere that are determined by mobilization and immobilization processes. Despite no clear treatment effect on average P flux in any spatial domain and no clear trends for P flux gradients, the slightly lower average rhizosphere P flux (Fig. 4c) as well as the darker areas in the P flux images around older root tissues (white arrows in Fig. 2) indicate the development of P depletion zones. As already discussed and despite the high sensitivity of DGT-LA-ICPMS (*i.e.,* low limits of detection), poor contact due to the presence of large pores, and a small share of root-free area within the small DGT-ROIs led to bulk soil values with a high variability. Moreover, averaging of old and young root sections and different root types could hamper the detection of P depletion zones. The size of a depletion zone around a root generally depends on the soil texture, P availability, age of the root (Hübel and Beck, 1993) and varies along the root, as P uptake is usually highest within the first cm from the tip (Colmer and Bloom, 1998; Fang et al., 2007; Marschner et al., 2011; Santner et al., 2012) and gradually decreases along the root axis as root hairs decrease (De Bauw et al., 2021; White et al., 2013). If replenishment of depletion zones around older and rather inactive root sections occurred over a longer period, depletion zones cannot be observed any more. This is favoured in soils having a high sorption capacity (Hübel and Beck, 1993) establishing new equilibrium conditions over time, which was likely the case in the loam. However, in sand the lower P binding on Al and Fe oxides, higher diffusion, and faster desorption kinetics (Menezes-Blackburn et al., 2016; Smolders et al., 2020) might also allow fast replenishment. Moreover, phosphate hydrolysed by phosphatases could also cause replenishment of depletion zones of older root sections, especially as phosphatases were homogenously distributed along the roots.

The observed high labile P flux on the root surface of young root tissues could originate either from the growing root itself or from the soil. Possible reasons could be P released from sloughed off cells as proposed by Santner et al. (2012) or P efflux from root tips which depends on P supply and was previously observed even under P deficient conditions (Cogliatti and María, 1990; Elliott et al., 1984). As DGT images visualize the result (i.e. labile P) of several processes occurring simultaneously, it is not possible to distinguish between individual processes.

4.5. Mn flux

Mn is highly sensitive to changes in pH and redox conditions in the rhizosphere (Husson, 2013; Rengel, 2015). Therefore, solubility of Mn in the rhizosphere might increase due to acidification or the exudation of organic compounds capable of complexing Mn. Even though we did not directly measure the redox potential, Mn solubility could be also increased by oxygen depletion caused by root and microbial respiration (Rengel, 2015; Sparrow and Uren, 1987). Moreover, soil organic matter mineralization in the rhizosphere by microorganisms, *i.e.*, oxidation, is often accompanied by Mn reduction which is optimal at pH 6–7 (Myers and Nealson, 1988), and can explain elevated rhizosphere Mn flux at sites of higher carbon (*e.g.* exudate) turnover and acidification. The often homogenous Mn distribution along the roots and the high degree of co-localization of phosphatase activity and Mn (70 ± 5%) on the root surface also suggests that we potentially analysed Mn present in acid phosphatases that might have bound to the DGT gel, as these metallo-enzymes consist of Fe^{3+}-Mn^{2+} centres (Carboni and Latour, 2011; Schenk et al., 2013) which are required co-factors for activation (Schmidt, 2019; Smith and Walker, 1991).

4.6. Interactions of P solubilization processes in the rhizosphere

Overlap coefficients for pH-phosphatase, pH-Mn and phosphatase-Mn on the root surface were in a similar range around 70% which suggests interactions of all 3 parameters as root-induced processes. The high co-occurrence of acidification and acid phosphatase hotspots indicates that protons released by roots shifted the pH optimum (*i.e.*, pH < 7) in favour for increased acid phosphatase activity (Dick et al., 2000). Even though average overlap coefficients of P flux hotspots with acidification or acid phosphatase hotspots were generally low on different root segments, root tips showed co-localized hotspots of acidification, phosphatase activity, P flux (Fig. S4), Mn flux (Fig. S4) and Zn flux (Fig. S6). The root tips and elongation zone growing into previously P-undepleted soil are more biochemically active than basal parts of the root and are thus the main contributors to overall P uptake (De Bauw et al., 2020). The co-occurrence of pH < 7 and elevated acid phosphatase activity is hence especially favourable at the major sites of P uptake, *i.e.*, young root tissues. Mn and Zn are often co-mobilized by P-deficiency-induced rhizosphere processes such as acidification and organic acids (Kreuzeder et al., 2018; Lambers et al., 2015; Neumann and Romheld, 2002). Co-localized P, Mn and Zn fluxes hence suggest that elevated P fluxes around root tips are at least partly derived from soil mobilization processes.

In sand, co-localization coefficients of acidification and acid

phosphatase activity were higher than in loam which is in line with the slightly higher hotspot coverage and (slightly) larger rhizosphere extents of both parameters in sand compared to patchier distribution along the roots in loam. The higher hotspot coverage of pH, acid phosphatase activity and Mn on the root surface in sand may indicate more pronounced root processes in response to P-limitation (*i.e.* lower total P and P_{CAL}, Table 1) or may be a result of less sorption or improved detection due to better sensor-soil contact in sand. Due to the higher amount of Ca-phosphates deriving from the fertilization in sand, acidification might be more important in terms of P solubilization because solubility of Ca-phosphates increases with lower pH (Penn and Camberato, 2019). But the effect of fertilization was likely restricted to the upper parts of the plots as the P fertilizer was surface applied and was limited as reflected by the generally lower P contents in maize grown on sand. The higher presence of organic P (Section S4) suggests that, in loam, acid phosphatase activity played a more prominent role in plant P nutrition compared to the sand. Due to the relatively short root hairs (0.24 mm; (Lippold et al., 2021), we did not observe a clear effect of root hairs on average rhizosphere extents of acidification and acid phosphatase activity. However, WT root tips were more acidic than *rth3* tips, potentially contributing to locally increased P solubility and uptake. As we could not observe increased P fluxes in WT (Figs. 2 and S4), the higher P contents in WT compared to *rth3* are most likely related to the higher absorption surface due to the presence of root hairs leading to greater P uptake despite similar extent and intensity of P solubilizing processes in the rhizosphere of both maize genotypes.

5. Conclusion & perspectives

For the first time, we visualized multiple P mobilization processes, *i.e.*, rhizosphere acidification, acid phosphatase activity as well as labile P and Mn *in situ* on and around field-grown maize roots at the transition of vegetative to reproductive growth (BBCH 59). Images showed a strong patchiness of root and rhizosphere hotspot activities/concentrations and a large variability between replicates, which necessitated elaborate image analysis. To obtain more robust results under field conditions, we suggest increasing particularly the number of applied DGT gels to at least 12–16 per treatment to increase the number of replicates suitable for analysis to 3–4, considering that only ¼ from the total applied DGTs were suitable for analysis in our study. This should be considered in experimental and financial planning of future field studies. Additionally, the area of the ROI should be larger to ensure that tips are not growing out of the ROI during application. Moreover, keeping the time between the individual methods as short as possible should provide more replicates suitable for co-localization analysis. Nevertheless, our novel strategy to integrate data of average rhizosphere gradients, average concentrations/activities within defined spatial domains (root surface, rhizosphere, bulk soil), hotspot coverage and co-localization within each domain and over different positions along the root axis enabled identification of root hair and substrate effects in the field.

We found average rhizosphere extents up to 1.6 mm for acidification, acid phosphatase activity and Mn flux, but could not define them for P depletion presumably due to the co-occurrence of P mobilizing processes and rapid P uptake. The presence of root-hairs (with a relatively short length of about 0.24 mm) did not significantly increase the average intensity or rhizosphere extent of any parameter, while the soil substrate, *i.e.*, texture and soil organic matter and the associated content of organic P, had a more pronounced impact. In sand average rhizosphere extents for acid phosphatase activity were ~1 mm larger, and average rhizosphere acidification showed steeper gradients and was ~0.1 pH units stronger than loam. We attribute these findings to the lower buffer capacity and more pronounced diffusion of solutes in the sand compared to loam. Furthermore, acidification was observed mainly around young root tissues (<2 cm from root cap) and wild-type tips were more acidic than tips of root-hair defective *rth3*. High P flux co-localized with acidification at root tips. Acidification was likely linked to root growth and created a pH optimum for acid phosphatase activity, (i.e., transformation of P_o to available phosphate) and P uptake especially at the root tips and within the elongation zone which are the major sites of P uptake. Due to the higher P availability, both genotypes grew better in loam than in sand; however, the presence of root hairs resulted in a higher P uptake and greater shoot biomass production of WT compared to *rth3*.

The combined imaging of phosphatase activity, soil pH and nutrient gradients *in situ* revealed that individual P solubilizing processes co-localized and interacted in the rhizosphere. Our results also demonstrate the challenge to find significant and clear trends under field conditions as several processes occur simultaneously, *i.e.*, mobilization, solubilization, desorption, enzymatic conversion of P_o to P_i, microbial mobilization, and immobilization as well as P uptake. P mobilization in the rhizosphere is thus often masked by competitive and rapid P uptake by roots and microbes. Moreover, different root types and changing parameter dynamics along the roots exhibited a large variability affecting average trends, which should be considered for modelling studies. Nevertheless, imaging techniques are non-destructive, can be applied *in situ* in both lab and field studies and can easily be coupled with other methods such as localized sampling for analysis of soil properties, microbes, or exudates to get a better understanding of soil-root-microorganism interactions. Our presented approach of stepwise integration of imaging data can also further be applied in nutrient cycling models and upscaling scenarios from the single root to (field) plot scale.

Declaration of competing interest

The authors declare that they have no known competing financial interests or personal relationships that could have appeared to influence the work reported in this paper.

Acknowledgments

This work was conducted within the framework of the priority program 2089, funded by the Deutsche Forschungsgemeinschaft (DFG, German Research Foundation) – Project numbers: 403803214 (E. Oburger & M. Santangeli), 403670038 (B.S. Razavi & S. Spielvogel), 403801423 (DV), 403640293 (D. Vetterlein & S. Schlüter). Seeds of the maize mutant *rth3* were provided by Caroline Marcon and Frank Hochholdinger (University of Bonn). An exchange between the universities of Kiel and Montpellier was funded by a German Academic Exchange Service (DAAD) scholarship (57445354, B.S. Razavi & I. Bertrand). G. Daudin and I. Bertrand received funding from Campus France (PHC PROCOPE 42609SH). C. Hummel was partly funded by Gesellschaft für Forschungsförderung Niederösterreich m.b.H. (SC17-015). J. Santner received funding from the Austrian Science Fund (FWF) and the Federal State of Lower Austria (P27571-BBL). E. Oburger was also supported by the European Research Council (ERC StG 801954 PhytoTrace). Authors gratefully acknowledge Gottfried Wieshammer from Technisches Büro für Bodenkultur, Austria (gottfried.wieshammer@aon.at) for his part in designing and constructing the root windows, as well as project coordinator Susanne Schreiter and Sebastian Häusler for their great organizational help during the application of our imaging methods in the field.

Appendix A. Supplementary data

Supplementary data to this article can be found online at https://doi.org/10.1016/j.soilbio.2021.108497.

References

Baldovinos, F., Thomas, G.W., 1967. The effect of soil clay content on phosphorus uptake. Soil Science Society of America Journal 1, 2–4. https://doi.org/10.2136/sssaj1967.03615995003100050020x.

Barrow, N.J., 2017. The effects of pH on phosphate uptake from the soil. Plant and Soil 410, 401–410. https://doi.org/10.1007/s11104-016-3008-9.

Barrow, N.J., Debnath, A., Sen, A., 2020. Measurement of the effects of pH on phosphate availability. Plant and Soil 454, 217–224. https://doi.org/10.1007/s11104-020-04647-5.

Bertrand, I., Hinsinger, P., Jaillard, B., Arvieu, J.C., 1999. Dynamics of phosphorus in the rhizosphere of maize and rape grown on synthetic, phosphated calcite and goethite. Plant and Soil 211, 111–119. https://doi.org/10.1023/A:1004328815280.

Bilyera, N., Zhang, X., Duddek, P., Fan, L., Banfield, C.C., Schlüter, S., Carminati, A., Kaestner, A., Ahmed, M.A., Kuzyakov, Y., Dippold, M.A., Spielvogel, S., Razavi, B.S., 2021. Maize genotype-specific exudation strategies: an adaptive mechanism to increase microbial activity in the rhizosphere. Soil Biology and Biochemistry 162, 108426. https://doi.org/10.1016/j.soilbio.2021.108426.

Bleiholder, H., Weber, E., Lancashire, P.D., Feller, C., Burh, L., Hess, M., Wicke, H., Hack, H., Meier, U., Klose, R., van den Boom, T., Strauss, R., 2001. Growth stages of mono-and dicotyledonous plants. In: Federal Biological Research Centre for Agriculture and Forestry, Second. BBCH Monograph.

Blossfeld, S., Gansert, D., 2007. A novel non-invasive optical method for quantitative visualization of pH dynamics in the rhizosphere of plants. Plant, Cell and Environment 30, 176–186. https://doi.org/10.1111/j.1365-3040.2006.01616.x.

Bolte, S., Cordelières, F.P., 2006. A guided tour into subcellular colocalization analysis in light microscopy. Journal of Microscopy. https://doi.org/10.1111/j.1365-2818.2006.01706.x.

Carboni, M., Latour, J.M., 2011. Enzymes with an heterodinuclear iron-manganese active site: curiosity or necessity? Coordination Chemistry Reviews 255, 186–202. https://doi.org/10.1016/j.ccr.2010.08.003.

Carter, M.R., Gregorich, E.G., 2007. Soil Sampling and Methods of Analysis, 2d ed. CRC Press, Boca Raton, FL, USA. https://doi.org/10.1201/9781420005271.

Cogliatti, D.H., María, G.E.S., 1990. Influx and efflux of phosphorus in roots of wheat plants in non-growth-limiting concentrations of phosphorus. Journal of Experimental Botany 41, 601–607. https://doi.org/10.1093/jxb/41.5.601.

Colmer, T.D., Bloom, A.J., 1998. A comparison of NH4+ and NO3- net fluxes along roots of rice and maize. Plant, Cell and Environment 21, 240–246. https://doi.org/10.1046/j.1365-3040.1998.00261.x.

Daly, K.R., Keyes, S.D., Masum, S., Roose, T., 2016. Image-based modelling of nutrient movement in and around the rhizosphere. Journal of Experimental Botany 67, 1059–1070. https://doi.org/10.1093/jxb/erv544.

De Bauw, P., Mai, T.H., Schnepf, A., Merckx, R., Smolders, E., Vanderborght, J., 2020. A functional-structural model of upland rice root systems reveals the importance of laterals and growing root tips for phosphate uptake from wet and dry soils. Annals of Botany 126, 789–806. https://doi.org/10.1093/aob/mcaa120.

De Bauw, P., Smolders, E., Verbeeck, M., Senthilkumar, K., Houben, E., Vandamme, E., 2021. Micro-dose placement of phosphorus induces deep rooting of upland rice. Plant and Soil. https://doi.org/10.1007/s11104-021-04914-z.

Dick, W.A., Cheng, L., Wang, P., 2000. Soil acid and alkaline phosphatase activity as pH adjustment indicators. Soil Biology and Biochemistry 32, 1915–1919. https://doi.org/10.1016/S0038-0717(00)00166-8.

Dinkelaker, B., Marschner, H., 1992. In vivo demonstration of acid phosphatase activity in the rhizosphere of soil-grown plants. Plant and Soil 144, 199–205. https://doi.org/10.1007/BF00012876.

Dong, S., Brooks, D., Jones, M.D., Grayston, S.J., 2007. A method for linking in situ activities of hydrolytic enzymes to associated organisms in forest soils. Soil Biology and Biochemistry 39, 2414–2419. https://doi.org/10.1016/j.soilbio.2007.03.030.

Elliott, G.C., Lynch, J., Läuchli, A., 1984. Influx and efflux of P in roots of intact maize plants: double-labeling with 32P and 33P. Plant Physiology 76, 336–341. https://doi.org/10.1104/pp.76.2.336.

Fang, Y.Y., Babourina, O., Rengel, Z., Yang, X.E., Pu, P.M., 2007. Spatial distribution of ammonium and nitrate fluxes along roots of wetland plants. Plant Science 173, 240–246. https://doi.org/10.1016/j.plantsci.2007.05.006.

Gahoonia, T.S., Nielsen, N.E., Joshi, P.A., Jahoor, A., 2001. A root hairless barley mutant for elucidating genetic of root hairs and phosphorus uptake. Plant and Soil 235, 211–219. https://doi.org/10.1023/A:1016252614393.

George, T.S., Giles, C.D., Menezes-Blackburn, D., Condron, L.M., Gama-Rodrigues, A.C., Jaisi, D., Lang, F., Neal, A.L., Stutter, M.I., Almeida, D.S., Bol, R., Cabugao, K.G., Celi, L., Cotner, J.B., Feng, G., Goll, D.S., Hallama, M., Krueger, J., Plassard, C., Rosling, A., Darch, T., Fraser, T., Giesler, R., Richardson, A.E., Tamburini, F., Shand, C.A., Lumsdon, D.G., Zhang, H., Blackwell, M.S.A., Wearing, C., Mezeli, M. M., Almås, Å.R., Audette, Y., Bertrand, I., Beyhaut, E., Boitt, G., Bradshaw, N., Brearley, C.A., Bruulsema, T.W., Ciais, P., Cozzolino, V., Duran, P.C., Mora, M.L., de Menezes, A.B., Dodd, R.J., Dunfield, K., Engl, C., Frazão, J.J., Garland, G., González Jiménez, J.L., Graca, J., Granger, S.J., Harrison, A.F., Heuck, C., Hou, E.Q., Johnes, P.J., Kaiser, K., Kjær, H.A., Klumpp, E., Lamb, A.L., Macintosh, K.A., Mackay, E.B., McGrath, J., McIntyre, C., McLaren, T., Mészáros, E., Missong, A., Mooshammer, M., Negrón, C.P., Nelson, L.A., Pfahler, V., Poblete-Grant, P., Randall, M., Seguel, A., Seth, K., Smith, A.C., Smits, M.M., Sobarzo, J.A., Spohn, M., Tawaraya, K., Tibbett, M., Voroney, P., Wallander, H., Wang, L., Wasaki, J., Haygarth, P.M., 2018. Organic phosphorus in the terrestrial environment: a perspective on the state of the art and future priorities. Plant and Soil 427, 191–208. https://doi.org/10.1007/s11104-017-3391-x.

Gerke, J., 2015. The acquisition of phosphate by higher plants: effect of carboxylate release by the roots. A critical review. Journal of Plant Nutrition and Soil Science 178, 351–364. https://doi.org/10.1002/jpln.201400590.

Grierson, P.F., Comerford, N.B., 2000. Non-destructive measurement of acid phosphatase activity in the rhizosphere using nitrocellulose membranes and image analysis. Plant and Soil 218, 49–57. https://doi.org/10.1023/a:1014985327619.

Guber, A., Kravchenko, A., Razavi, B.S., Uteau, D., Peth, S., Blagodatskaya, E., Kuzyakov, Y., 2018. Quantitative soil zymography: mechanisms, processes of substrate and enzyme diffusion in porous media. Soil Biology and Biochemistry 127, 156–167. https://doi.org/10.1016/j.soilbio.2018.09.030.

Hager, A., 2003. Role of the plasma membrane H+-ATPase in auxin-induced elongation growth: historical and new aspects. Journal of Plant Research 116, 483–505. https://doi.org/10.1007/s10265-003-0110-x.

Hahn, G., Marschner, H., 1998. Effect of acid irrigation and liming on root growth of Norway spruce. Plant and Soil 199, 11–22.

Hinsinger, P., 2001. Bioavailability of soil inorganic P in the rhizosphere as affected by root-induced chemical changes: a review. In: Plant and Soil, pp. 173–195. https://doi.org/10.1023/A:1013351617532.

Hinsinger, P., Plassard, C., Tang, C., Jaillard, B., 2003. Origins of root-mediated pH changes in the rhizosphere and their responses to environmental constraints: a review. Plant and Soil 248, 43–59. https://doi.org/10.1023/A:1022371130939.

Hochholdinger, F., Wen, T.-J., Zimmermann, R., Chimot-Marolle, P., da Costa e Silva, O., Bruce, W., Lamkey, K.R., Wienand, U., Schnable, P.S., 2008. The maize (Zea mays L.) roothairless3 gene encodes a putative GPI-anchored, monocot-specific, COBRA-like protein that significantly affects grain yield. The Plant Journal 54, 888–898. https://doi.org/10.1111/j.1365-313X.2008.03459.x.

Hochholdinger, F., Woll, K., Sauer, M., Dembinsky, D., 2004. Genetic dissection of root formation in maize (Zea mays) reveals root-type specific developmental programmes. Annals of Botany 93, 359–368. https://doi.org/10.1093/aob/mch056.

Hochholdinger, F., Yu, P., Marcon, C., 2018. Genetic control of root system development in maize. Trends in Plant Science 23, 79–88. https://doi.org/10.1016/j.tplants.2017.10.004.

Holz, M., Zarebanadkouki, M., Carminati, A., Becker, J.N., Spohn, M., 2020. The effect of root hairs on rhizosphere phosphatase activity. Journal of Plant Nutrition and Soil Science 1–7. https://doi.org/10.1002/jpln.201900426, 000.

Huang, Q., Liang, W., Cai, P., 2005. Adsorption, desorption and activities of acid phosphatase on various colloidal particles from an Ultisol. Colloids and Surfaces B: Biointerfaces 45, 209–214. https://doi.org/10.1016/j.colsurfb.2005.08.011.

Hübel, F., Beck, E., 1993. In-situ determination of the P-relations around the primary root of maize with respect to inorganic and phytate-P. Plant and Soil 157, 1–9. https://doi.org/10.1007/bf00038742.

Hummel, C., Boitt, G., Santner, J., Lehto, N.J., Condron, L., Wenzel, W.W., 2021. Co-occurring increased phosphatase activity and labile P depletion in the rhizosphere of Lupinus angustifolius assessed with a novel, combined 2D-imaging approach. Soil Biology and Biochemistry 153. https://doi.org/10.1016/j.soilbio.2020.107963.

Husson, O., 2013. Redox potential (Eh) and pH as drivers of soil/plant/microorganism systems: a transdisciplinary overview pointing to integrative opportunities for agronomy. Plant and Soil 362, 389–417. https://doi.org/10.1007/s11104-012-1429-7.

Itoh, S., Barber, S.A., 1983. A numerical solution of whole plant nutrient uptake for soil-root systems with root hairs. Plant and Soil 70, 403–413. https://doi.org/10.1007/BF02374895.

Jones, D.L., 1998. Organic acids in the rhizosphere – a critical review. Plant and Soil 205, 25–44. https://doi.org/10.1023/A:1004356007312.

Jones, D.L., Oburger, E., 2011. Solubilization of phosphorus by soil microorganisms. In: Bünemann, E., Oberson, A., Frossard, E. (Eds.), Phosphorus in Action, Soil Biology. Springer Berlin Heidelberg, Berlin, Heidelberg, pp. 215–243. https://doi.org/10.1007/978-3-642-15271-9.

Jungk, A., 2001. Root hairs and the acquisition of plant nutrients from soil. Journal of Plant Nutrition and Soil Science 164, 121–129. https://doi.org/10.1002/1522-2624, 200104)164:2<121::AID-JPLN121>3.0.CO;2-6.

Kandeler, E., Marschner, P., Tscherko, D., Singh Gahoonia, T., Nielsen, N.E., 2002. Microbial community composition and functional diversity in the rhizosphere of maize. Plant and Soil 238, 301–312. https://doi.org/10.1023/A:1014479220689.

Kreuzeder, A., Santner, J., Prohaska, T., Wenzel, W.W., 2013. Gel for simultaneous chemical imaging of anionic and cationic solutes using diffusive gradients in thin films. Analytical Chemistry 85, 12028–12036. https://doi.org/10.1021/ac403050f.

Kreuzeder, A., Santner, J., Scharsching, V., Oburger, E., Hoefer, C., Hann, S., Wenzel, W. W., 2018. In situ observation of localized, sub-mm scale changes of phosphorus biogeochemistry in the rhizosphere. Plant and Soil 424, 573–589. https://doi.org/10.1007/s11104-017-3542-0.

Kuzyakov, Y., Razavi, B.S., 2019. Rhizosphere size and shape: temporal dynamics and spatial stationarity. Soil Biology and Biochemistry 135, 343–360. https://doi.org/10.1016/J.SOILBIO.2019.05.011.

Lambers, H., Hayes, P.E., Oliveira, R.S., Laliberte, E., Turner, B.L., 2015. Leaf manganese accumulation and phosphorus-acquisition efficiency. Trends in Plant Science. https://doi.org/10.1016/j.tplants.2014.10.007.

Lippold, E., Phalempin, M., Schlüter, S., Vetterlein, D., 2021. Does the lack of root hairs alter root system architecture of Zea mays? Plant and Soil. https://doi.org/10.1007/s11104-021-05084-8.

Lucas, M., Schlüter, S., Vogel, H., Vetterlein, D., 2019. Roots compact the surrounding soil depending on the structures they encounter. Scientific Reports 9, 16236. https://doi.org/10.1038/s41598-019-52665-w.

Ma, X., Liu, Y., Shen, W., Kuzyakov, Y., 2021. Phosphatase activity and acidification in lupine and maize rhizosphere depend on phosphorus availability and root properties

: coupling zymography with planar optodes. Applied Soil Ecology 167, 104029. https://doi.org/10.1016/j.apsoil.2021.104029.
Ma, X., Zarebanadkouki, M., Kuzyakov, Y., Blagodatskaya, E., Pausch, J., Razavi, B.S., 2018. Spatial patterns of enzyme activities in the rhizosphere: effects of root hairs and root radius. Soil Biology and Biochemistry 118, 69–78. https://doi.org/10.1016/j.soilbio.2017.12.009.
Majda, M., Robert, S., 2018. The role of auxin in cell wall expansion. International Journal of Molecular Sciences 19. https://doi.org/10.3390/ijms19040951.
Manzoor, M., Abbasi, M.K., Sultan, T., 2017. Isolation of phosphate solubilizing bacteria from maize rhizosphere and their potential for rock phosphate solubilization–mineralization and plant growth promotion. Geomicrobiology Journal 34, 81–95. https://doi.org/10.1080/01490451.2016.1146373.
Marschner, H., Häussling, M., George, E., 1991. Ammonium and nitrate uptake rates and rhizosphere pH in non-mycorrhizal roots of Norway spruce [Picea abies (L.) Karst. Trees 5, 14–21. https://doi.org/10.1007/BF00225330.
Marschner, P., Crowley, D., Rengel, Z., 2011. Rhizosphere interactions between microorganisms and plants govern iron and phosphorus acquisition along the root axis - model and research methods. Soil Biology and Biochemistry 43, 883–894. https://doi.org/10.1016/j.soilbio.2011.01.005.
Mehra, O.P., Jackson, M.L., 1960. Iron oxide removal from soils and clays by a dithionite-citrate system buffered with sodium bicarbonate. Proc. 7th Nat. Conf. Clays. 317–327.
Menezes-Blackburn, D., Zhang, H., Stutter, M., Giles, C.D., Darch, T., George, T.S., Shand, C., Lumsdon, D., Blackwell, M., Wearing, C., Cooper, P., Wendler, R., Brown, L., Haygarth, P.M., 2016. A holistic approach to understanding the desorption of phosphorus in soils. Environmental Science & Technology 50, 3371–3381. https://doi.org/10.1021/acs.est.5b05395.
Merbach, W., Deubel, A., Gransee, A., Ruppel, S., Klamroth, A.-K., 2010. Phosphorus solubilization in the rhizosphere and its possible importance to determine phosphate plant availability in soil. A review with main emphasis on German results. Archives of Agronomy and Soil Science 56, 119–138. https://doi.org/10.1080/03650340903005640.
Myers, C.R., Nealson, K.H., 1988. Bacterial manganese reduction and growth with manganese oxide. Science 240, 1319–1321.
Neumann, G., George, T.S., Plassard, C., 2009. Strategies and methods for studying the rhizosphere-the plant science toolbox. Plant and Soil 321, 431–456. https://doi.org/10.1007/s11104-009-9953-9.
Neumann, G., Romheld, V., 2002. Root-induced changes in the ability of nutrients in the rhizosphere. In: Waisel, Y., Eshel, A., Kafkafi, U. (Eds.), Plant Roots–The Hidden Half. Marcel Dekker, Inc., New York, pp. 617–649.
Oburger, E., Schmidt, H., 2016. New methods to unravel rhizosphere processes. Trends in Plant Science 21, 243–255. https://doi.org/10.1016/j.tplants.2015.12.005.
Olagoke, F.K., Kaiser, K., Mikutta, R., Kalbitz, K., Vogel, C., 2020. Persistent activities of extracellular enzymes adsorbed to soil minerals. Microorganisms 8, 1–15. https://doi.org/10.3390/microorganisms8111796.
Olagoke, F.K., Kalbitz, K., Vogel, C., 2019. Control of soil extracellular enzyme activities by clay minerals—perspectives on microbial responses. Soil Systems 3, 1–16. https://doi.org/10.3390/soilsystems3040064.
Olesen, T., Moldrup, P., Yamaguchi, T., Rolston, D.E., 2001. Constant slope impedance factor model for predicting the solute diffusion coefficient in unsaturated soil. Soil Science 166, 89–96. https://doi.org/10.1097/00010694-200102000-00002.
Penn, C.J., Camberato, J.J., 2019. A critical review on soil chemical processes that control how soil ph affects phosphorus availability to plants. Agriculture 9, 1–18. https://doi.org/10.3390/agriculture9060120.
Petersen, W., Böttger, M., 1991. Contribution of organic acids to the acidification of the rhizosphere of maize seedlings. Plant and Soil 132, 159–163. https://doi.org/10.1007/BF00010396.
Pierzynski, G.M., McDowell, R.M., Sims, J.T., 2005. Chemistry, cycling, and potential movement of inorganic phosphorus in soils. In: Phosphorus: Agriculture and the Environment. American Society of Agronomy, pp. 53–86.
Prjanischnikow, D., 1929. Zur Frage nach der Ammoniak Ernährung von höheren Pflanzen. Biochimische Zeitschrift 227, 341–349.
Raymond, N.S., Gómez-Muñoz, B., Bom, F.J.T., Nybroe, O., Jensen, L.S., Müller-Stöver, D.S., Oberson, A., Richardson, A.E., 2020. Phosphate-solubilising microorganisms for improved crop productivity: a critical assessment. New Phytologist nph 16924. https://doi.org/10.1111/nph.16924.
Razavi, B.S., Zarebanadkouki, M., Blagodatskaya, E., Kuzyakov, Y., 2016. Rhizosphere shape of lentil and maize: spatial distribution of enzyme activities. Soil Biology and Biochemistry 79, 229–237. https://doi.org/10.1016/j.soilbio.2016.02.020.
Razavi, B.S., Zhang, X., Bilyera, N., Guber, A., Zarebanadkouki, M., 2019. Soil zymography: simple and reliable? Review of current knowledge and optimization of the method. Rhizosphere. https://doi.org/10.1016/j.rhisph.2019.100161.
Rengel, Z., 2015. Availability of Mn, Zn and Fe in the rhizosphere. Journal of Soil Science and Plant Nutrition 15, 397–409. https://doi.org/10.4067/s0718-95162015005000036.
Rudolph-Mohr, N., Tötzke, C., Kardjilov, N., Oswald, S.E., 2017. Mapping water, oxygen, and pH dynamics in the rhizosphere of young maize roots. Journal of Plant Nutrition and Soil Science 180, 336–346. https://doi.org/10.1002/jpln.201600120.
Ruiz, S., Koebernick, N., Duncan, S., Fletcher, D.M., Scotson, C., Boghi, A., 2020. Significance of Root Hairs at the Field Scale – Modelling Root Water and Phosphorus Uptake under Different Field Conditions, pp. 281–304.
Santner, J., Zhang, H., Leitner, D., Schnepf, A., Prohaska, T., Puschenreiter, M., Wenzel, W.W., 2012. High-resolution chemical imaging of labile phosphorus in the rhizosphere of Brassica napus L. cultivars. Environmental and Experimental Botany 77, 219–226. https://doi.org/10.1016/j.envexpbot.2011.11.026.
Schenk, G., Mitić, N.Š., Hanson, G.R., Comba, P., 2013. Purple acid phosphatase: a journey into the function and mechanism of a colorful enzyme. Coordination Chemistry Reviews 257, 473–482. https://doi.org/10.1016/j.ccr.2012.03.020.
Schindelin, J., Arganda-Carreras, I., Frise, E., Kaynig, V., Longair, M., Pietzsch, T., Preibisch, S., Rueden, C., Saalfeld, S., Schmid, B., Tinevez, J.-Y., White, D.J., Hartenstein, V., Eliceiri, K., Tomancak, P., Cardona, A., 2012. Fiji: an open-source platform for biological-image analysis. Nature Methods 9, 676–682. https://doi.org/10.1038/nmeth.2019.
Schmidt, Husted, 2019. The biochemical properties of manganese in plants. Plants 8, 381. https://doi.org/10.3390/plants8100381.
Schüller, H., 1969. Die CAL-Methode, eine neue Methode zur Bestimmung des pflanzenverfügbaren Phosphates in Böden. Zeitschrift für Pflanzenernährung und Bodenkunde 123, 48–63. https://doi.org/10.1002/jpln.19691230106.
Schwertmann, U., 1964. Differenzierung der Eisenoxide des Bodens durch Extraktion mit Ammoniumoxalat-Lösung. Zeitschrift Für Pflanzenernährung, Düngung, Bodenkunde 105, 194–202. https://doi.org/10.1002/jpln.3591050303.
Sims, J., Pierzynski, G., 2005. Chemistry of phosphorus in soil. In: Tabatabai, A., Sparks, D. (Eds.), Chemical Processes in Soil, SSSA Book Series 8. SSSA, Madison, pp. 151–192.
Smith, R.D., Walker, J.C., 1991. Isolation and expression of a maize type 1 protein phosphatase. Plant Physiology 97, 677–683. https://doi.org/10.1104/pp.97.2.677.
Smolders, E., Nawara, S., De Cooman, E., Merckx, R., Martens, S., Elsen, A., Odeurs, W., Vandendriessche, H., Santner, J., Amery, F., 2020. The phosphate desorption rate in soil limits phosphorus bioavailability to crops. European Journal of Soil Science. https://doi.org/10.1111/ejss.12978.
Sorrell, B.K., Orr, P.T., 1993. H + exchange and nutrient uptake by roots of the emergent hydrophytes, Cyperus involucratus Rottb., Eleocharis sphacelata R. Br. and Juncus ingens N. A. Wakef. New Phytologist 125, 85–92. https://doi.org/10.1111/j.1469-8137.1993.tb03866.x.
Sparrow, L.A., Uren, N.C., 1987. Oxidation and reduction of Mn in acidic soils: effect of temperature and soil pH. Soil Biology and Biochemistry 19, 143–148. https://doi.org/10.1016/0038-0717(87)90073-3.
Spohn, M., Carminati, A., Kuzyakov, Y., 2013. Soil zymography - a novel in situ method for mapping distribution of enzyme activity in soil. Soil Biology and Biochemistry 58, 275–280. https://doi.org/10.1016/j.soilbio.2012.12.004.
Stober, C., George, E., Persson, H., 2000. Root Growth and Response to Nitrogen, pp. 99–121. https://doi.org/10.1007/978-3-642-57219-7_5.
Stutter, M.I., Shand, C.A., George, T.S., Blackwell, M.S.A., Bol, R., MacKay, R.L., Richardson, A.E., Condron, L.M., Turner, B.L., Haygarth, P.M., 2012. Recovering phosphorus from soil: a root solution? Environmental Science & Technology 46, 1977–1978. https://doi.org/10.1021/es2044745.
Turner, B.L., Driessen, J.P., Haygarth, P.M., Mckelvie, I.D., 2003. Potential contribution of lysed bacterial cells to phosphorus solubilisation in two rewetted Australian pasture soils. Soil Biology and Biochemistry 35, 187–189. https://doi.org/10.1016/S0038-0717(02)00244-4.
Turner, B.L., Mckelvie, I.D., Haygarth, P.M., 2002. Characterisation of water-extractable soil organic phosphorus by phosphatase hydrolysis. Soil Biology and Biochemistry 34, 27–35.
Vetterlein, D., Lippold, E., Schreiter, S., Phalempin, M., Fahrenkampf, T., Hochholdinger, F., Marcon, C., Tarkka, M., Oburger, E., Ahmed, M., Javaux, M., Schlüter, S., 2021. Experimental platforms for the investigation of spatiotemporal patterns in the rhizosphere—laboratory and field scale. Journal of Plant Nutrition and Soil Science 184, 35–50. https://doi.org/10.1002/jpln.202000079.
Wagner, S., Hoefer, C., Prohaska, T., Santner, J., 2020. Two-dimensional visualization and quantification of labile, inorganic plant nutrients and contaminants in soil. Journal of Visualized Experiments. https://doi.org/10.3791/61661.
Wen, T.-J., Schnable, P.S., 1994. Analyses of mutants of three genes that influence root hair development in Zea mays (gramineae) suggest that root hairs are dispensable. American Journal of Botany 81, 833. https://doi.org/10.2307/2445764.
Whipps, J.M., 2001. Microbial interactions and biocontrol in the rhizosphere. Journal of Experimental Botany 52, 487–511. https://doi.org/10.1093/jxb/52.suppl_1.487.
White, P.J., George, T.S., Gregory, P.J., Bengough, A.G., Hallett, P.D., McKenzie, B.M., 2013. Matching roots to their environment. Annals of Botany 112, 207–222. https://doi.org/10.1093/aob/mct123.
Yang, Y., Wang, N., Guo, X., Zhang, Y., Ye, B., 2017. Comparative analysis of bacterial community structure in the rhizosphere of maize by high throughput pyrosequencing. PLoS One 12, 1–11. https://doi.org/10.1371/journal.pone.0178425.